Bioresource Technology 460 (2026) 135330

Contents lists available at ScienceDirect

Bioresource Technology

journal homepage: www.elsevier.com/locate/biortech

Flow-driven structural and transcriptomic responses in syntrophic electroactive biofilms

Mahshid Golalikhani, Ahmed Elreedy *, Benjamin Fritz, René Wurst, Christian Jonas Lapp, Johannes Gescher *

Institute of Technical Microbiology, Hamburg University of Technology, Hamburg 21073, Germany

HIGHLIGHTS

- Raising flow velocity tripled co-culture biofilm density and current 2.5-fold.
- *G. sulfurreducens* monocultures stay flow-insensitive; syntrophy drives response.
- *S. oneidensis* shapes biofilm architecture despite under 5% of transcript reads.
- *bpfD* upregulated 10.7-fold under shear governs connectivity and current output.
- *bpfD*-deletion lowered current 7.5-fold, confirming gene-regulated shear response.

GRAPHICAL ABSTRACT

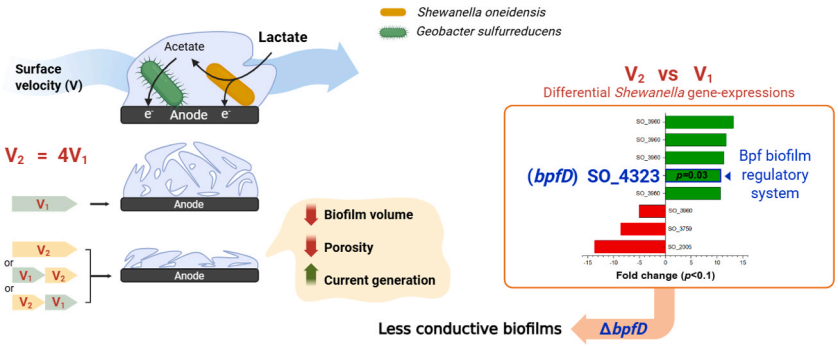

ARTICLE INFO

Keywords:
Bioelectrochemical systems
Hydrodynamic shear stress
Surface velocity
Anodic biofilms
Porosity
bpfD

ABSTRACT

Bioelectrochemical systems (BES) are versatile platforms for energy and resource recovery, where electroactive biofilms serve as the key biocatalyst. While performance depends on flow dynamics, the interplay between hydrodynamic conditions, biofilm architecture, and gene-regulation in syntrophic communities remains poorly understood. We investigated defined surface flow velocities (0.2 and 0.8 mm/s) on the structure and electroactivity of *Shewanella oneidensis–Geobacter sulfurreducens* coculture biofilms. Higher flow produced more compact biofilms with lower biovolume and porosity, yielding higher current densities. Flow transitions induced persistent structural and electrochemical shifts, indicating an adaptive, gene-regulated response to shear. Since *G. sulfurreducens* monoculture biofilms were flow-insensitive, regulation appears to originate from *S. oneidensis*. Transcriptomics showed strong shear response, including 10.7-fold upregulation of *bpfD*. Its deletion reduced current density and increased porosity despite comparable biovolume. Three-dimensional fluorescence in situ hybridization imaging revealed a porous, loosely organized structure within the mutant biofilm. This was consistent with the structural and electrochemical differences observed. These findings reveal that community-level electrochemical performance can be governed by a minor transcriptional contributor rather than by the dominant current-producing species.

* Corresponding authors.
E-mail addresses: ahmed.elreedy@tuhh.de (A. Elreedy), johannes.gescher@tuhh.de (J. Gescher).

https://doi.org/10.1016/j.biortech.2026.135330
Received 20 May 2026; Received in revised form 13 June 2026; Accepted 4 July 2026
Available online 7 July 2026

1. Introduction

Electroactive biofilms in bioelectrochemical systems (BESs) are formed by exoelectrogenic microorganisms that colonize electrode surfaces, utilizing them as terminal electron acceptors to sustain their metabolism (Kokko et al., 2018). *Shewanella oneidensis* and *Geobacter sulfurreducens* are well-established model exoelectrogens with complementary metabolic and biofilm-forming properties. Their syntrophic interaction is based on lactate conversion by *S. oneidensis* and subsequent acetate utilization by *G. sulfurreducens,* thereby expanding the substrate range for anodic current production, as previously shown by E. Klein et al. (2023). At the same time, the two organisms differ markedly in their extracellular electron transfer strategies and biofilm-forming capabilities. Therefore, this coculture provides a suitable model system to investigate how flow dynamics affect the structure, composition, and electrochemical performance of syntrophic electroactive biofilms.

Hydrodynamic conditions play a central role in regulating biofilm development and activity in flow-through systems (Xiao et al., 2021). Flow velocity and flow regime determine substrate delivery, removal of metabolic byproducts, and mass transport across the biofilm–liquid interface, thereby shaping bacterial attachment, nutrient diffusion, and biofilm growth dynamics (Alotaibi, 2021; Wang et al., 2022). In BESs, hydrodynamic shear force is a key factor shaping electroactive biofilm architecture and electrochemical output (Rago et al., 2016). Previous studies have shown that low shear stress can lead to the formation of thick, heterogeneous biofilms with metabolically active outer layers and inactive, nutrient-depleted cores, ultimately limiting electron transfer and reducing current generation (Islam et al., 2019). Conversely, excessive shear stress may exceed biofilm adhesion and cohesion forces, causing detachment of cells, extracellular polymeric substances (EPS), or entire biofilm clusters, thereby compromising long-term stability (Pizzi et al., 2025). Balanced shear stress mitigates diffusion limitation at low flow velocity and detachment at high flow velocity. Under these conditions, biofilms establish faster, reach higher cell densities, and exhibit higher metabolic activity (Godain et al., 2024; Jadhav and Ghangrekar, 2009).

Biofilm formation is mainly regulated by three systems: quorum sensing, intracellular second messengers, and two-component systems (Feng et al., 2021; Tang et al., 2025). Intracellular second messengers regulate bacterial physiology in response to external environmental signals, such as shear stress, and thereby control biofilm formation and properties (Fang et al., 2023; Tan et al., 2020). Cyclic diguanylate monophosphate (c-di-GMP) is a central second messenger that controls the planktonic–sessile transition by regulating motility, EPS production, and biofilm maturation (Elgamoudi et al., 2022; Liu et al., 2016). High intracellular c-di-GMP generally promotes attachment and matrix formation as it promotes adhesin and exopolysaccharide matrix production and suppresses motility, whereas low c-di-GMP favors motility and dispersal (Guo et al., 2017; Hengge, 2009; Park and Sauer, 2022). Shear stress can directly modulate c-di-GMP signaling. Fang et al. (2023) reported that small shear changes caused large c-di-GMP fluctuations in mixed-culture biofilms. Consistent with this, studies on electroactive biofilms demonstrate that shear stress directly influences anodic biofilm development by modulating biofilm thickness, density, and metabolic rate, thereby affecting both biofilm growth kinetics and electrochemical performance (Godain et al., 2024; Jones and Buie, 2019). To the best of our knowledge, there is currently limited information on the correlation between shear stress and intracellular c-di-GMP signaling in electroactive biofilms, and it remains unclear how this relationship may differ depending on biofilm growth mechanisms and the microorganisms involved.

This gap is especially pronounced for syntrophic coculture systems, in which one species supplies the substrate that sustains current generation by another, so that performance depends on the spatial coupling between partners rather than on the biomass of a single organism. Such interspecies dependence adds a layer of regulatory complexity that is rarely addressed. Here, we investigate how hydrodynamic conditions shape the structure, function, and molecular regulation of syntrophic electroactive coculture biofilms formed by *S. oneidensis* and *G. sulfurreducens*. To address these aims, we used a microfluidic BES combined with optical coherence tomography (OCT), which enable noninvasive, real-time monitoring of electroactive biofilm development under defined flow velocities and controlled shear transitions. Biofilm performance was evaluated by correlating current density with structural parameters, including biovolume and porosity. Transcriptomic analyses and targeted gene inactivation were used to understand molecular responses to shear stress. Together, these complementary approaches were chosen to provide mechanistic insight into how hydrodynamic forces regulate the structure and activity of a syntrophic electroactive biofilm.

2. Materials and Methods

2.1. Microfluidic BES

The electrochemical experiments were conducted in a custom-designed microfluidic BES flow cell, developed based on the protocol described by E. Klein et al. (2024a) (Supplementary Fig. S1). The setup integrates electrodes made from a graphite-polypropylene composite (PPG 86, Eisenhuth GmbH & Co. KG, Germany) with a projected surface area of 3 × 10 mm, embedded within the microchannel. The system consists of two microfluidic channels connected in series. The upstream microfluidic reactor contained the working electrode (i.e., anode) alongside a custom-fabricated Ag/AgCl reference electrode. The downstream microfluidic reactor held the counter electrode (i.e., cathode). Each microfluidic reactor has a total volume of 354 µL; three separate upstream and downstream microreactors were used, enabling triplicate measurements (Supplementary Fig. S2). Anaerobic conditions were provided to the upstream anodic reactors, gathered in one closed compartment, by continuous flushing with a gas mixture of 80% N_2 and 20% CO_2, whereas the cathodic reactors remain open to air. The electrode potentials were regulated by a SensorStat potentiostat (Uniscan Instruments Ltd, UK), which was connected to the electrodes via 0.1 mm silver foil (Chempur, Germany). The anodic potential was set at 0 V versus the standard hydrogen electrode. Chronoamperometry was used to continuously record current production at a fixed anodic potential, providing a suitable method for direct, non-disruptive monitoring of biofilm function during biofilm growth. Before inoculation, electrodes were sterilized with 70% (v/v) ethanol, and sterile growth medium was subsequently flushed through the system. Flow velocities of 0.2 and 0.8 mm/s were investigated using flow rates of 4 and 16 ml/h, corresponding to shear rates of 0.5 and 2.2 s^{-1} and shear stresses of 0.4 and 1.7 mPa, respectively. As the medium composition was kept identical at both velocities, the 4-fold higher flow rate corresponds to a proportionally higher volumetric organic loading rate. These velocities were chosen as two defined reference points, 0.2 mm/s matching the prior coculture study by E. Klein et al. (2024a) on this platform and 0.8 mm/s a 4-fold increase, rather than as a graded dose–response series.

2.2. Strains and growth conditions

S. oneidensis MR-1 (wild type) and the mutant strain MR-1Δ*bpfD*, as well as G. sulfurreducens PCA, were pre-cultured in growth medium following the protocol described by E. Klein et al. (2024a). For coculture experiments, the overnight cultures of S. oneidensis and G. sulfurreducens were mixed in a ratio of 10:1 and adjusted to an optical density (OD_{600}) of 4.0. This ratio was selected to ensure sufficient acetate production from lactate by S. oneidensis to support G. sulfurreducens growth. For single-culture experiments, inocula were prepared identically and adjusted to an OD_{600} of 4. As shown in Supplementary Fig. S2, inoculation was done through the side port of the microfluidic reactor using a syringe pump (L160, Landgraf Laborsysteme HLL GmbH) at 2

mL/h for 2 h; at the same time, the medium flow was supplied at 2 mL/h through the front port using peristaltic pumps (Reglo ICC, ISMATEC Industry Solutions GmbH). After inoculation, the inoculum supply was stopped, and the medium flow rate was adjusted to the respective experimental flow rate of either 4 or 16 mL/h.

2.3. Transcriptomic analysis and stop-codon integration

RNA was isolated from anodic biofilm cocultures of *S. oneidensis* and *G. sulfurreducens* using the RNeasy PowerBiofilm kit (Qiagen, Hilden, Germany) according to the manufacturer's instructions. Library prep and Illumina sequencing were conducted by Eurofins Genomics (Ebersberg, Germany). A strand-specific library of cDNA was prepared and sequenced with a target of 50 million read pairs (2 × 150 bp) per sample. A biological triplicate was prepared for each experimental condition. All raw sequencing data can be accessed through NCBI via SRA accession PRJNA1444911. Stop codon integration was carried out using a CRISPR/dCas9 as previously described by Fritz et al. (2025) to generate targeted gene mutations. The primers, oligonucleotides, and plasmid used are provided in Supplementary Tables S1 and S2, and Supplementary Fig. S3.

2.4. Fluorescence in situ hybridization (FISH)

An automated FISH procedure was performed as previously described by E. Klein et al. (2024a). The probes SHEW227 (5′-[6-FAM]-AGC TAA TCC CAC CTA GGT WCA TC-3′) and GEO2 (5′-[Cyanine 3]-GAA GAC AGG AGG CCC GAA A-3′) were used for the detection of S. oneidensis and G. sulfurreducens, respectively. Images were acquired using a Nikon Ti2 spinning disk confocal microscope (Nikon Instruments Inc., Melville, NY, USA) equipped with a SoRa (Super-Resolution Airy) unit and a TIRF (Total Internal Reflection Fluorescence) module. The relative abundances of S. oneidensis and G. sulfurreducens were quantified using Fiji (ImageJ, version 2.1.0/1.53). For quantitative analysis, images were converted to 8-bit format and binarized using an appropriate threshold (0–255).

2.5. Analytical methods and calculations

Biofilm mesostructure was characterized using optical coherence tomography (OCT) with a GANYMEDE-II spectral-domain system (Thorlabs GmbH, Dachau, Germany) equipped with an LSM04 objective. Imaging parameters followed the protocol described by Bauer et al. (2019). Acquired datasets were processed using ImageJ/FIJI software (version 2.1.0/1.53). Biomass was distinguished from background by applying an intensity threshold and binarizing the images, in which white pixels counted as biofilm and black pixels as background. Biofilm volume (biovolume) was calculated by correlating the number of image pixels with the respective voxel sizes (voxel dimensions of 4 × 4 × 2.14 μm (x/y/z)). The height maps of the biofilm were generated using the image-processing routine developed by Wagner and Horn (2017). Biofilm porosity (%) was calculated by comparing the measured biofilm actual height (h) to the normalized height that is equally distributed over the anode surface area, according to Equation (1). Biomass was distinguished from void in the binarized OCT stack, with strongly backscattering signal classified as biofilm. The actual height (h_actual) is the average biofilm height referenced to the anode, and the normalized height (h_normalized) is the biovolume divided by the projected image area, that is the height the same biomass would occupy if distributed evenly across the electrode. As the biofilm is uneven, h_actual exceeds h_normalized, and porosity expresses the fraction of the occupied height envelope not filled by biomass, at the resolution of the OCT system. This height-based metric differs from the conventional volumetric void fraction and does not describe internal pore connectivity.

The current density (I) was calculated by dividing the measured current i (μA) by the projected surface area (SA; cm^2) of the working electrode (Equation (2). The mean current density ($\bar{I}$) over an experimental period was calculated by dividing the integrated current density (I) by the corresponding experimental time (t) (Equation (3). The relative abundance and cell fraction (%) for each species were calculated using Equations (4) and (5), where $P_{whitepixels,i}$ is the number of white pixels corresponding to the respective species and $\sum P_{whitepixels}$ is the total number of white pixels assigned to both species.

$$\text{Porosity } (\%) = \frac{h_{actual} - h_{normalized}}{h_{actual}} \times 100 \quad (1)$$

$$I = \frac{i}{SA} \quad (2)$$

$$\text{Mean current density} = \frac{\int_0^t Idt}{t} \quad (3)$$

$$\text{Relative abondance of cells} = \frac{P_{\text{white pixels,i}}}{\sum P_{\text{white pixels}}} \times 100 \quad (4)$$

$$\text{Cell fraction} = \frac{P_{\text{white,i}}}{\sum P_{\text{(white+black pixels)}}} \times 100 \quad (5)$$

Principal components analysis (PCA) was conducted, as a multivariate analysis tool, to study the impact of velocity dynamics on various performance parameters, i.e., biofilm volume, porosity, and current density, using JMP 19 (Student Edition).

3. Results and discussion

3.1. Flow velocity shapes biofilm architecture–performance balance

A coculture of *G. sulfurreducens* and *S. oneidensis* was grown in microfluidic bioelectrochemical flow cells to investigate the influence of flow velocity on biofilm characteristics and current density. Biofilm development and current density were monitored over time at two flow velocities, 0.2 and 0.8 mm/s. The effect of flow velocity was evaluated over time, and both the time-course data and the corresponding mean current densities are shown in Fig. 1. Current density was recorded until a stable phase was reached under each condition, by day 8 at 0.2 mm/s and day 6 at 0.8 mm/s. For direct comparison over the same time window, Fig. 1 presents the overlapping period between both conditions, while the complete low-flow profile, which reached a stable phase by day 8, is shown in Fig. S4 (Supplementary). As shown in Fig. 1a, biofilms grown at a flow velocity of 0.8 mm/s initiated current production earlier and achieved a higher mean current density (86.3 μA/cm^2) compared to those grown at 0.2 mm/s (34.1 μA/cm^2). Systems operated at 0.8 mm/s also achieved the current plateau earlier, by day 6. In contrast, biofilms formed at 0.2 mm/s exhibited slightly higher biovolume (Fig. 1b) and significantly greater porosity (17.1%). Because the 0.2 mm/s biofilms had already reached comparable or higher biovolume without comparable current output, we do not expect that longer operation alone would cause the current densities to converge. Biofilms grown at 0.8 mm/s were notably denser, with a porosity of only 5.3%, confirming the formation of thinner biofilms under this condition.

In the coculture studied here, *S. oneidensis* oxidizes lactate to acetate, which subsequently serves as a substrate for *G. sulfurreducens*. Under comparable porosity and external flow conditions, a thinner biofilm may reduce diffusion limitations for acetate, flavins, protons, and other metabolites within the biofilm, facilitating metabolite and electron exchange between the two species, as reported by Jones and Buie (2019). In addition, excessive porosity may increase the separation between these two microorganisms and from the electrode (Pham et al., 2008; Yang et al., 2019). In summary, the lower flow velocity (0.2 mm/s) produced more porous biofilm structures and lower current densities, despite the slightly higher overall biovolume. Conversely, the higher flow rate (0.8 mm/s) produced denser biofilm architectures that

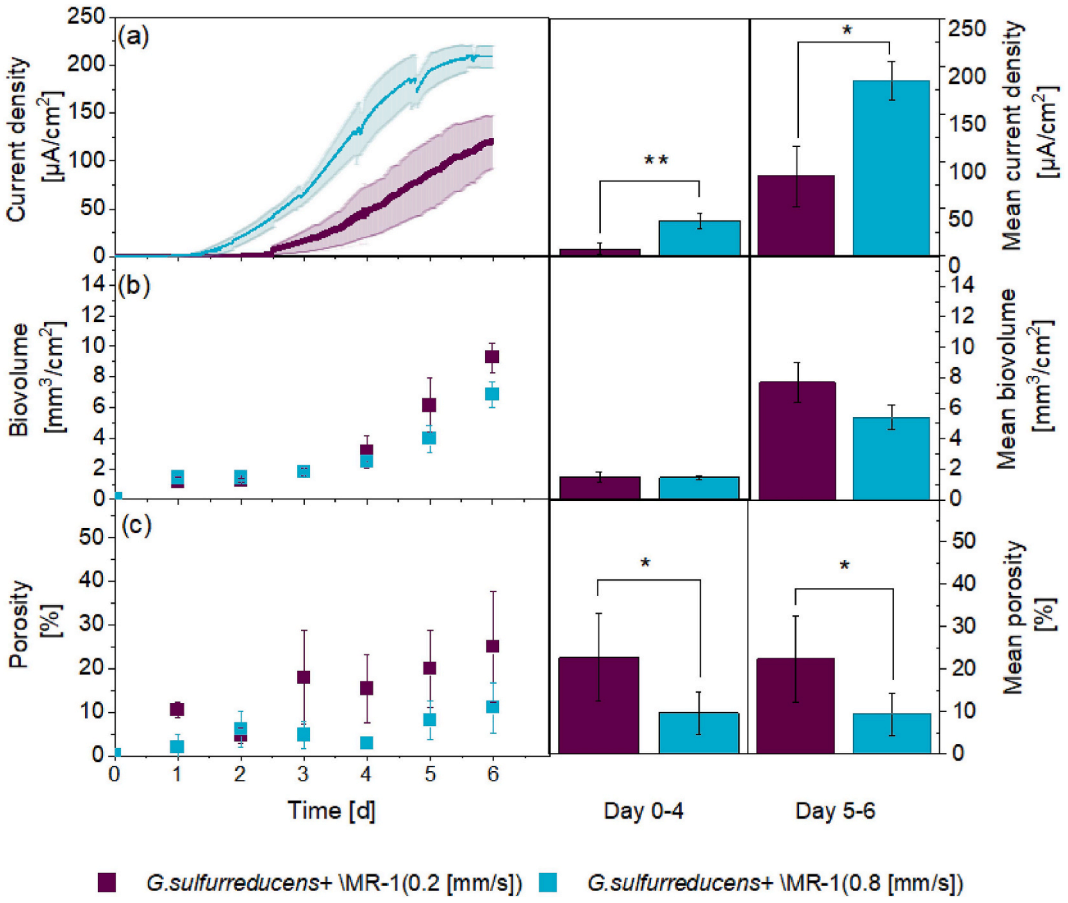

Fig. 1. Biofilm development and electrochemical performance of *G. sulfurreducens–S. oneidensis* MR-1 cocultures under flow velocities of 0.2 and 0.8 mm/s. (a) current density, (b) biovolume, and (c) porosity over time on the left side, with corresponding mean values on the right side. Statistical significance: * = $p < 0.05$; ** = $p < 0.01$.

catalyzed significantly higher current densities. The inverse relationship between porosity and current density reflects the syntrophic nature of the system rather than classical bulk-substrate diffusion. While higher porosity may facilitate substrate transport from the bulk liquid, current production in this coculture depends mainly on close interspecies exchange between S. *oneidensis* and *G. sulfurreducens*. Thus, the more porous biofilm formed at 0.2 mm/s likely increased interspecies distances and weakened syntrophic coupling, whereas the denser biofilm formed at 0.8 mm/s favored local metabolite exchange and electron transfer, resulting in higher current densities.

The results are in agreement with previous studies. Thick biofilms were revealed to reduce electrochemical performance because of diffusion limitations and inactive biomass regions (Gomes and Mergulhão, 2021), while elevated shear promotes compactness, increases biofilm density, and improves electrochemical performance (Kugaprasatham et al., 1992; Van Loosdrecht et al., 2002). These observations raised the question of whether the effect of flow velocity on biofilm structure is purely mechanical or whether higher flow velocity additionally triggers biological adaptations that alter cellular regulatory mechanisms governing biofilm formation. To fundamentally address this question, we first reduced the complexity of the biofilm and repeated the experiment using a pure culture of *G. sulfurreducens* supplied with acetate as the carbon and electron source to elucidate whether both strains would be affected by flow velocity. Thereby, we eliminated the dependence on the catabolic activity of *S. oneidensis*.

Pure cultures of *G. sulfurreducens* exhibited a markedly different phenotype compared to the coculture. *G. sulfurreducens* showed minimal differences between the two flow velocities. Current density remained comparable at 0.2 and 0.8 mm/s. Similarly, biovolume and porosity showed minimal variation between the two conditions (Supplementary Fig. S6). The results are also in line with the findings of Jones (2018), which showed no significant changes in biofilm thickness and surface roughness for *G. sulfurreducens* at shear stress of 0.01 and 1 Pa. Although the applied shear stresses in the present study were substantially lower than those reported by them, their observation under different shear conditions is qualitatively consistent with the limited morphological response observed for G. sulfurreducens in our system.

Since G. *sulfurreducens* biofilm architecture appears intrinsically insensitive to the flow regimes tested, the hydrodynamic regulation of coculture biofilm structure is unlikely to originate from G. *sulfurreducens* and more likely involves *S. oneidensis*. A direct test using a *S. oneidensis* monoculture is not informative, since *S. oneidensis* alone generates very low current and forms a biofilm below the detection limit of OCT (E. Klein et al., 2024a). This attribution is instead consistent with the syntrophic, lactate-based metabolism of the coculture, in which *G. sulfurreducens* relies on acetate supplied by *S. oneidensis,* so that *S. oneidensis* governs the substrate transfer that sustains current. Because the medium was identical at both velocities, *G. sulfurreducens* monoculture experienced the same 4-fold increase in volumetric organic loading rate, yet its current density and biofilm structure did not change. This indicates that the main current producer was not loading-limited over this range, so the higher loading rate alone does not account for the velocity-dependent response of the coculture. It is examined directly in the following sections, where transcriptomic profiling and targeted gene deletion provide positive evidence that *S. oneidensis* mediates the response. This would imply that a species contributing only a minor share of the biomass and transcriptional output may nonetheless influence the structural and functional properties of the entire community.

3.2. Response of developing coculture biofilms to flow velocity shift

If modulation of biofilm chemistry occurs in response to flow conditions, leading to different biofilm characteristics, this difference should be longer-lasting and not easily reversible by changes in flow velocity. To test this hypothesis, we grew coculture biofilms for four days in six independent microfluidic reactors under the higher flow rate of 0.8 mm/s, then switched three of the reactors to the lower flow rate of 0.2 mm/s on day four. Fig. S7 (supplementary) shows the results of this analysis. Reducing the flow velocity from 0.8 to 0.2 mm/s resulted in only minor changes compared to biofilms grown at a constant 0.8 mm/s. In Phase 2, mean current density slightly decreased from 185.2 to 157.1 μA/cm^2, biovolume changed only slightly from 5.4 to 5.0 mm^3/cm^2, and porosity increased modestly from 9.1 to 10.4%. Data acquisition continued until the current reached a steady state in either of the tested conditions, which defined the experimental endpoint, so that the analysis reflects biofilm responses during the growth phase rather than long-term behaviour. Within this window, the biofilms retained the low-porosity architecture established under high flow rather than reverting toward the constant low-flow phenotype, although the modest rise in porosity indicates that further structural changes beyond this window cannot be excluded. Moreover, the comparable current density and biovolume observed after reducing the flow velocity, suggest that substrate-flux limitation alone was not the dominant driver of the observed biofilm response in Fig. 1.

At this point in the experimental series, we knew that only coculture biofilms of *S. oneidensis* and *G. sulfurreducens* were affected by flow-velocity modulation, whereas *G. sulfurreducens* pure cultures did not show a similar pattern. Moreover, the persistent structure and functionality of the two-species biofilm after a switch in flow rate pointed toward a regulatory program changing biofilm matrix composition rather than toward solely flow-velocity-dependent compression of the biofilm. Nevertheless, it was also possible that time frame after the flow rate switch was insufficient for biofilm rearrangements to occur. Therefore, we conducted the experiment in reverse, starting with a low flow rate in six individual microfluidic BES reactors and then switching to a higher flow velocity after four days in three of the reactors. The results are depicted in Fig. 2. When the flow velocity increased from 0.2 to 0.8 mm/s, biofilms responded differently compared to those maintained at constant low flow (0.2 mm/s). After the shift, the mean current density rose to 151.3 μA/cm^2, significantly higher than the 98.1 μA/cm^2 observed under constant low flow. Biovolume, however, was lower in the shifted condition, reaching only 2.4 mm^3/cm^2, compared to 9.1 mm^3/cm^2 under constant low flow. Porosity also decreased substantially from 30.3% to 9.7%, indicating a denser biofilm.

In summary, the experimental duration was clearly sufficient to cause a change in biofilm structure and functionality. Within four days, both biofilm characteristics began to diverge progressively, with lower porosity and higher current density emerging as hallmarks of biofilms after the switch to a higher flow rate (Fig. 2). To better visualize the relationships among biofilm volume, porosity, and current density under all tested conditions, PCA was conducted separately after the first and second phases (Supplementary Fig. S8). In both analyses, PC1 and PC2 together explained more than 99% of the total variance. After the first phase, clear clustering according to the two flow velocities was observed. After the second phase, the conditions involving changes from 0.8 to 0.2 mm/s and from 0.2 to 0.8 mm/s clustered together with the constant 0.8 mm/s condition and were distinct from the constant 0.2

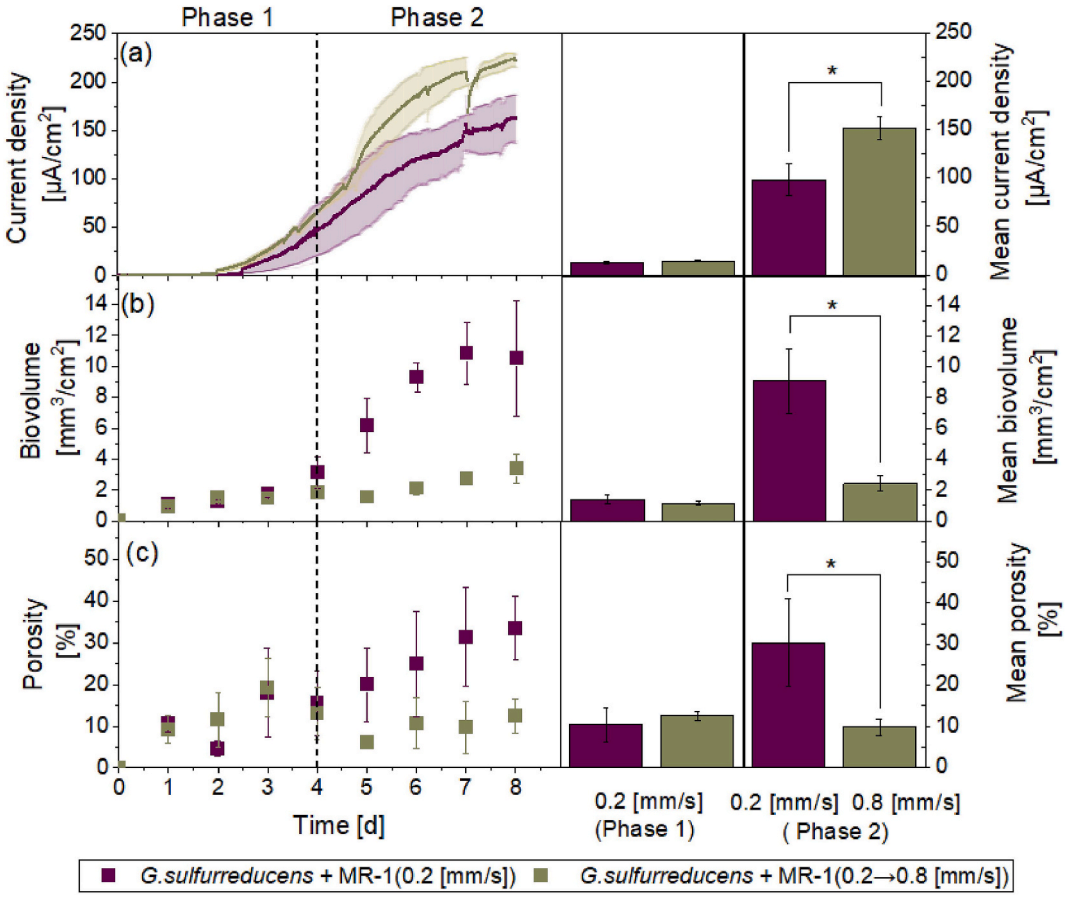

Fig. 2. Effect of flow velocity (constant 0.2 mm/s versus varied velocity from 0.2 to 0.8 mm/s) on *G. sulfurreducens–S. oneidensis* coculture biofilms. (a) current density, (b) biovolume, and (c) porosity over time on the left side, with corresponding mean values on the right side. Statistical significance: *= $p < 0.05$; **=$p < 0.01$.

mm/s condition. In addition, the corresponding loading plots highlight a shift in the relationship between biofilm volume and current density: it was positive after the first phase (early biofilm) and became negative after the second phase.

3.3. Transcriptomic evidence for gene-regulated response to hydrodynamic stress

As evidence from the previous experiments pointed towards a regulatory response of foremost *S. oneidensis* cells to shear stress, a transcriptomic analysis was performed on coculture biofilms cultivated at constant flow velocities of 0.2 and 0.8 mm/s. The relative transcriptional activity was compared between the two flows at days 4 and 6 or 8, correlating with active biofilm growth and steady state conditions, respectively. *G. sulfurreducens* was the dominant contributor to transcriptomic reads under all conditions, showing only a slight decrease in activity at higher flow rates and steady state. In contrast, *S. oneidensis* exhibited a strong flow-dependent response, with low and declining activity at 0.2 mm/s but increased gene expression at 0.8 mm/s (Table S3, supplementary). These results indicate that while *G. sulfurreducens* kept having the by far dominant relative gene expressions across hydrodynamic regimes, the *S. oneidensis* transcriptomic activity had more relative sensitivity to flow dynamics and increased relatively to *G. sulfurreducens* when increasing flow velocity, suggesting that transcriptional regulation by this species plays a key role in the observed flow-dependent biofilm behavior. The increased relative gene expression of *S. oneidensis* at higher flow velocity (0.8 mm/s) likely supports an induced adaptive regulatory response, either to shear stress or to an increased metabolic rate resulting from lower mass transfer limitation, as previously suggested by Jones and Buie (2019).

Not only did overall transcriptomic activity change due to increased flow velocity, but also the expression of individual genes after 4 days for biofilms grown under flow velocities of 0.2 and 0.8 mm/s. This phase also corresponds to the stage when strain-specific differences in biofilm formation were most evident. A total of 83 genes showed differential expression between biofilms grown under 0.2 mm/s and 0.8 mm/s, with 98.6% belonging to *S. oneidensis* (Supplementary Table S4 and Fig. S9). These results again emphasize the stronger transcriptional response of *S. oneidensis* to increases in flow conditions during the early stages of biofilm development. The eight *S. oneidensis* genes exhibiting the highest significant expression differences ($p < 0.1$, fold change > 5) between the two applied flow velocities are shown in Table 1. The threshold of $p < 0.1$ was chosen as the relative number of reads for *S. oneidensis* in the coculture was rather low (0.8 to 4.1%) and a more restrictive filtering substantially reduced the candidate gene pool. Meanwhile, the resulting list served as a screening step to identify a target for genomic mutation, and the gene ultimately selected, *bpfD,* met a more stringent significance level.

Cyclic-di-GMP was in many organisms, including *S. oneidensis,* revealed to be a major regulatory contributor to biofilm development (Chao et al., 2013; Thormann et al., 2006). Among the top differentially expressed genes, SO_4323, which encodes the EAL domain-containing protein (i.e., *bpfD*), and SO_3759, encoding a sensor-domain diguanylate cyclase (i.e., *dgc*), exhibited opposite transcriptional responses to flow velocity and both interact with cyclic-di-GMP. Comparing expression levels of biofilms grown at 0.8 mm/s with those at 0.2 mm/s, *bpfD* expression was strongly upregulated (+10.67-fold), whereas *dgc* expression was markedly downregulated (–8.67-fold). To understand the potential contribution of these two genes' regulations, it was previously discussed that the EAL-domain in BpfD was revealed to be in fact not catalytically active in cyclic-di-GMP hydrolysis but a binding domain leading via several steps to BpfA exposure to the cell surface, where this protein connects cells with each other (Zhou et al., 2015). In addition, Zhou et al. (2015) found that BpfD is likely responsible for BpfA (which is responsible for cell–cell connections) release and export to the cell surface in an interplay with BpfG, and its deletion caused strong defects in biofilm formation in pure cultures of *S. oneidensis*. Hence, we hypothesize that the coordinated regulation of *bpfD* and *dgc* likely contributes to the change in biofilm structure and efficiency, particularly the *S. oneidensis* fraction, in response to flow velocity, thereby optimizing the coculture biofilm performance. Notably, *bpfD* was selected for targeted deletion because it was among the most strongly flow-responsive genes in our transcriptomic data, rather than because of its general role in biofilm formation. The deletion strain was then tested under both flow conditions to assess whether the functional impact of *bpfD* on biofilm architecture and current differs with the hydrodynamic regime. As it was not possible to overexpress *dgc* using a plasmid system, as this would necessitate antibiotic selection pressure that would lead to *G. sulfurreducens* death, we decided to study biofilm development in a clean *bpfD* deletion strain.

Additionally, it is noteworthy that several of the differentially expressed genes can be linked with previous works from our research group, i.e., Edel et al. (2021) and Klein et al. (2025). For instance, the upregulated expression of SO_3271, an UDP-*N*-acetylglucosamine 4,6-dehydratase, and SO_3191, a Wzz/FepE/Etk *N*-terminal domain-containing protein, aligns with the polysaccharide changes by overexpression of WbpA (UDP-*N*-acetyl-D-glucosamine 6-dehydrogenase) and WbpP (UDP-*N*-acetyl-D-glucosamine 6-dehydrogenase) and their impact on biofilm architecture and current production. Upregulation of SO_3271 promotes GlcNAc modification for flagella and capsule branches. Likewise, elevated SO_3191 extends O-antigen chains, enhancing envelope rigidity; this activation, alongside upregulated precursors (WbpP, RmlA), might direct resources toward expanded polysaccharide matrices, strengthening adhesion and structural integrity for improved electroactivity (Klein et al., 2025; Kolker et al., 2005; Kouzuma et al., 2010).

Table 1
List of the highest differentially expressed genes, with *p*-value below 0.1, identified in the coculture biofilm when subjected to different flow velocities.

Name	Function	Fold change	*p*-value
SO_2005	TraR/DksA C4-type zinc finger protein	−13.68	0.09
SO_3759	**Sensor domain-containing diguanylate cyclase (*dgc*)**	**−8.67**	**0.08**
SO_3960	LPS export ABC transporter ATP-binding protein	−5.09	0.06
SO_3271	UDP-*N*-acetylglucosamine 4,6-dehydratase (inverting)	10.66	0.03
SO_4323	**EAL domain-containing protein (*bpfD*)**	**10.67**	**0.03**
SO_1531	tRNA uracil 4-sulfurtransferase ThiI	11.33	0.02
SO_2956	phage tail tube protein	11.77	0.002
SO_3191	Wzz/FepE/Etk *N*-terminal domain-containing protein	13.16	0.05

3.4. Role of candidate gene SO_4323 (bpfD) in biofilm response to flow velocity

Results are presented for the 0.8 → 0.2 mm/s flow velocity transition in Fig. 3, and for the 0.2 → 0.8 mm/s flow velocity transition in Fig. 4. Cocultures with MR-1Δ*bpfD* produce significantly lower current densities compared to those with wild-type *S. oneidensis* MR-1. In Phase 1, the mutant produced a mean current density of 5.2 μA/cm^2, approximately 7.5 times lower than the wild type (39.5 μA/cm^2). In Phase 2, this difference remained substantial, with the mutant reaching 38.5 μA/cm^2 compared to 157.1 μA/cm^2 for the wild type. Despite the reduced electrochemical activity, the mutant formed biofilms with higher biovolume, 2.8 mm^3/cm^2 vs. 1.8 mm^3/cm^2 in Phase 1, and 8.6 mm^3/cm^2 vs. 5.0 mm^3/cm^2 in Phase 2. Porosity was also higher in the mutant, with values of 6.7% compared to 4.4% in Phase 1, and 19.3% compared to 10.2% in Phase 2. Interestingly, while the wild type seemed to keep biovolume and porosity almost constant after the switch to 0.2 mm/s, the mutant constantly increased biovolume and porosity. The biofilm

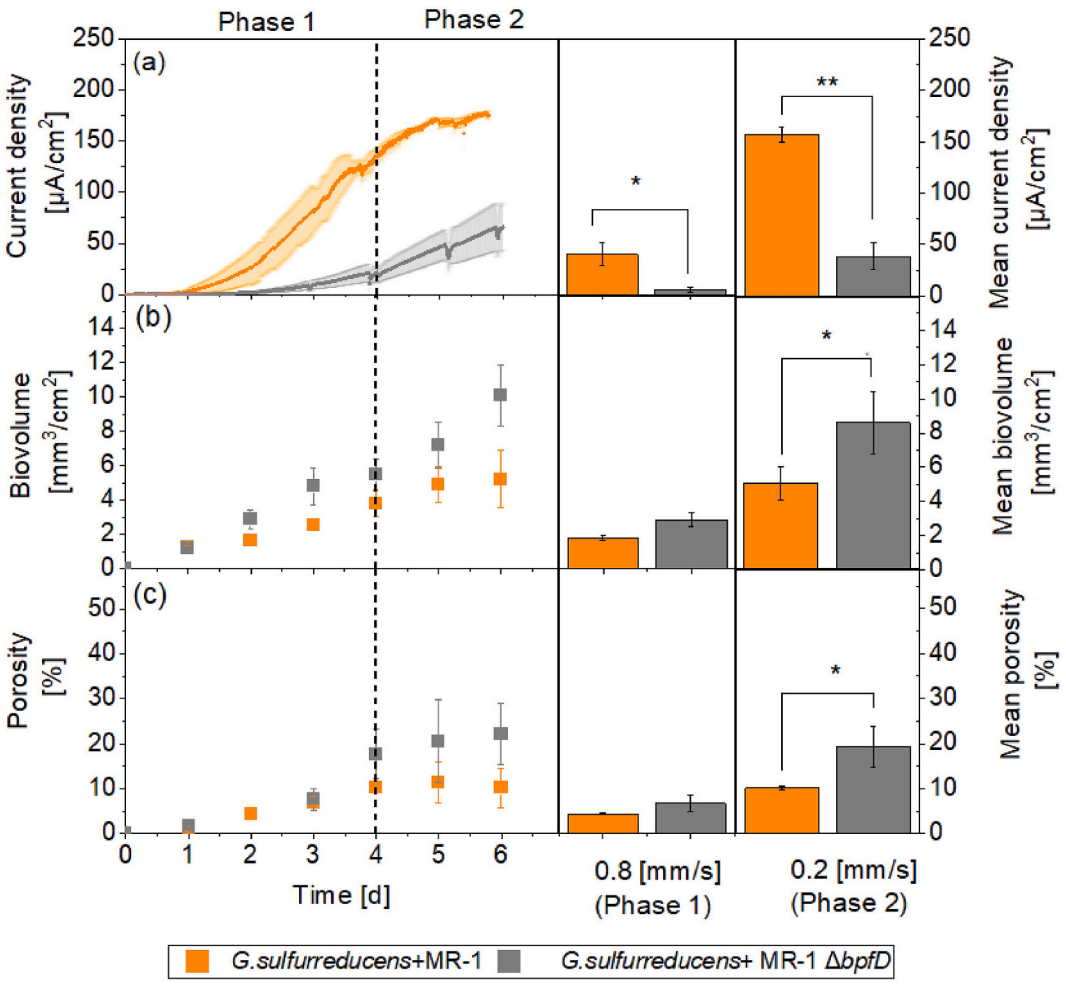

Fig. 3. Effect of decreasing flow velocity from 0.8 to 0.2 mm/s on electrochemical performance and biofilm structure in cocultures. Biofilms of *G. sulfurreducens*– *S. oneidensis* MR-1 and *G. sulfurreducens*–MR-1Δ*bpfD* were compared under identical flow conditions: Phase 1 (0.8 mm/s) and Phase 2 (0.2 mm/s). (a) current density, (b) biovolume, and (c) porosity over time on the left side, with corresponding mean values on the right side. Statistical significance: *= $p < 0.05$; **= $p < 0.01$.

heightmaps of both cocultured biofilms additionally emphasize this difference (Supplementary Fig. S10).

As the biovolume was similar at the end of phase 1, but the current density was lower by the mutant, it might be the case that less active cells and higher EPS content contributed to the observed biovolume. Less conductive EPS content has been reported to negatively influence the electroactivity of *S. oneidensis* biofilms (Gao et al., 2019; Mahto and Das, 2022). For example, biofilms with a lower EPS-to-protein ratio have been associated with increased current output in this microorganism (Gao et al., 2019; Kitayama et al., 2017). Although the Δ*bpfD* mutant formed biofilms with higher porosity, particularly after phase 2, no significant difference in porosity was observed after phase 1. Under initial high shear stress, the mutant biofilm appeared unable to compact or reinforce its matrix after the transition to lower flow velocity, resulting in a bulky and poorly conductive structure. Despite similar biovolume and porosity after phase 1, the observed differences in current density indicate that biofilm structure, while important, is not the sole determinant of electrochemical performance.

Fig. 4 shows the response of cocultures to an increase in flow velocity from 0.2 to 0.8 mm/s. In phase 1, the wild-type coculture reached a mean current density of 14.3 μA/cm^2, while the *bpfD* mutant reached 3.1 μA/cm^2. In phase 2, current densities increased to 151.3 μA/cm^2 for the wild type and 81.1 μA/cm^2 for the mutant. Biovolume remained comparable between cocultures in both phases, with 1.1 and 1.0 mm^3/cm^2 in phase 1, and 2.4 and 2.3 mm^3/cm^2 in phase 2 for the wild type and mutant, respectively. The corresponding biofilm heightmaps are shown in Supplementary Fig. S11. As shown in Fig. 4c, porosity was similar in Phase 1 (12.5% and 14.7%), but in phase 2, the mutant biofilms showed a much higher mean porosity of 32.9% compared with 9.7% for the wild type. It is noteworthy that porosity significantly differed between wild type and mutant in phase 2 which, based on our transcriptomic analysis, supports the potential role of increased *bpfD* expression on achieving denser biofilm. Although whole-genome sequencing was not performed, previous deep-sequencing analyses of the Target-AID platform in our laboratory did not detect off-target events, and the intended premature stop codon was confirmed by Sanger sequencing. Given that *bpfD* was strongly regulated and that the observed phenotype was consistent with its predicted biofilm-related function, we consider it unlikely that the effect resulted from a random background mutation.

Altogether, in coculture biofilms, the mutant consistently exhibited lower current densities than the wild-type. This electrochemical impairment occurred regardless of the specific flow velocities applied or the resulting variations in total biofilm volume. Because the mutant and wild type were compared under matched flow conditions, this difference cannot be attributed to shear or mass-transfer effects, and instead reflects a gene-dependent contribution to the response. Meanwhile, the reduction in current production is likely attributed to the structural properties of the mutant biofilm matrix. Planktonic growth assays of *S. oneidensis* showed no significant differences between the mutant and wild-type strains (Supplementary Fig. S12), indicating that the *bpfD* deletion does not affect basic cell viability. Hence, we hypothesize that the deletion of *bpfD* resulted in reduced cell–cell/cell-surface

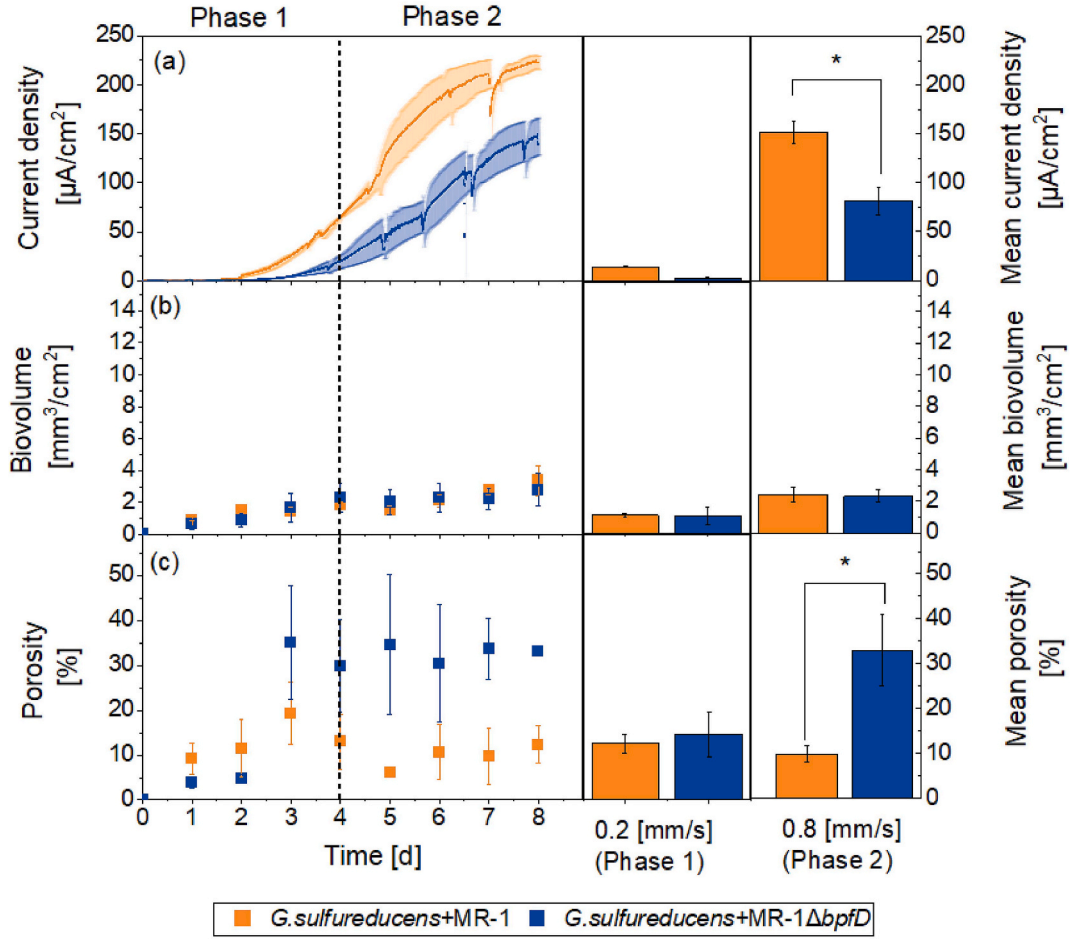

Fig. 4. Effect of increasing flow velocity from 0.2 to 0.8 mm/s on electrochemical performance and biofilm structure in cocultures. Biofilms of *G. sulfurreducens–S. oneidensis* MR-1 and *G. sulfurreducens*– MR-1Δ*bpfD* were compared under identical flow conditions: Phase 1 (0.2 mm/s) and Phase 2 (0.8 mm/s). (a) current density, (b) biovolume, and (c) porosity over time on the left side with corresponding mean values on the right side. Statistical significance: *= $p < 0.05$; **=$p < 0.01$.

concentrations of the BpfA connector, leading to increased biofilm porosity, possibly combined with overproduction of less-conductive EPS (this can additionally lead to an overestimated effective biofilm volume by means of OCT). Such structural changes would be expected to decrease the effective conductivity of the biofilm and increase the spatial separation between syntrophic cells, potentially limiting the efficiency of interspecies electron and metabolite transfer (Jadhav et al., 2019; E. Klein et al., 2024b; Lin et al., 2017; Matsumoto et al., 2021; Thormann et al., 2006). This interpretation is consistent with the biofilm-electroactivity values (i.e., mean current generated per unit biofilm volume (μA/cm^3); Supplementary Fig. S13), which were significantly lower in the mutant biofilms; additionally, the lower electroactivity of mutant biofilm at 0.8 → 0.2 mm/s compared with 0.2 → 0.8 mm/s suggests a higher necessity for robust adhesion/conductivity at elevated shearing force. These observations align with previous microfluidic studies of *S. oneidensis* pure cultures, where bpfA overexpression or specific mutations (e.g., bpfG C116S) led to increased adhesion and higher current densities (E. M. Klein et al., 2024b).

3.5. Cells distribution within the bpfD mutant biofilm

Spatial distribution and relative abundance of cells were analyzed by FISH combined with confocal laser scanning microscopy (CLSM) on mature coculture biofilms of G. sulfurreducens and MR-1Δ*bpfD* grown at the end of the experiment, where velocity changed from 0.8 to 0.2 mm/s (Fig. 5a–c and Supplementary Fig. S14). Quantification was performed by pixel-based analysis of binarized CLSM images using FISH signal intensity, which correlates with ribosome abundance. The relative abundance of *G. sulfurreducens* increased with biofilm depth (Fig. 5a). In contrast, *S. oneidensis* decreased and was mainly detected in the outer biofilm regions, as also illustrated in the 3D image (Fig. 5c). The upper biofilm layers (0 to − 5 μm) show an approximately similar distribution of both organisms. With increasing proximity to the anode, this balance shifted toward *G. sulfurreducens*. Thus, the final steps of electron transfer are likely dominated by *G. sulfurreducens*. The relative abundance of *S. oneidensis* measured here by FISH, from approximately 50% in the outer layers to 30–35% near the anode, reflects cell presence in the upper biofilm and should not be read as its share of community transcriptional activity. Cells represented only ~ 16–30% of the total imaged volume across all depths (Fig. 5b). This indicates that most of the biofilm volume is non-cellular, consisting of EPS and water-filled voids, which is in line with the low-conductivity, EPS-rich matrix inferred for the mutant. This is consistent with the OCT-derived porosity of ~ 22.1% in mature biofilm, which corresponds to water-filled voids. Together, the cell fraction and porosity account for less than two-thirds of the total biofilm volume, with the remainder attributable to EPS matrix, consistent with EPS constituting the dominant volume fraction of bacterial biofilms (Flemming, 2016).

The relative abundance of *G. sulfurreducens* compared to *S. oneidensis* near the anode surface was less than that reported by E. Klein et al. (2024a) for wild-type cocultures (65% and 35% vs 88% and 12%). This wild-type reference was obtained in the same laboratory using the same microfluidic system, wild-type strains, and FISH analysis procedure as the present study, with both biofilms analyzed at the end of the

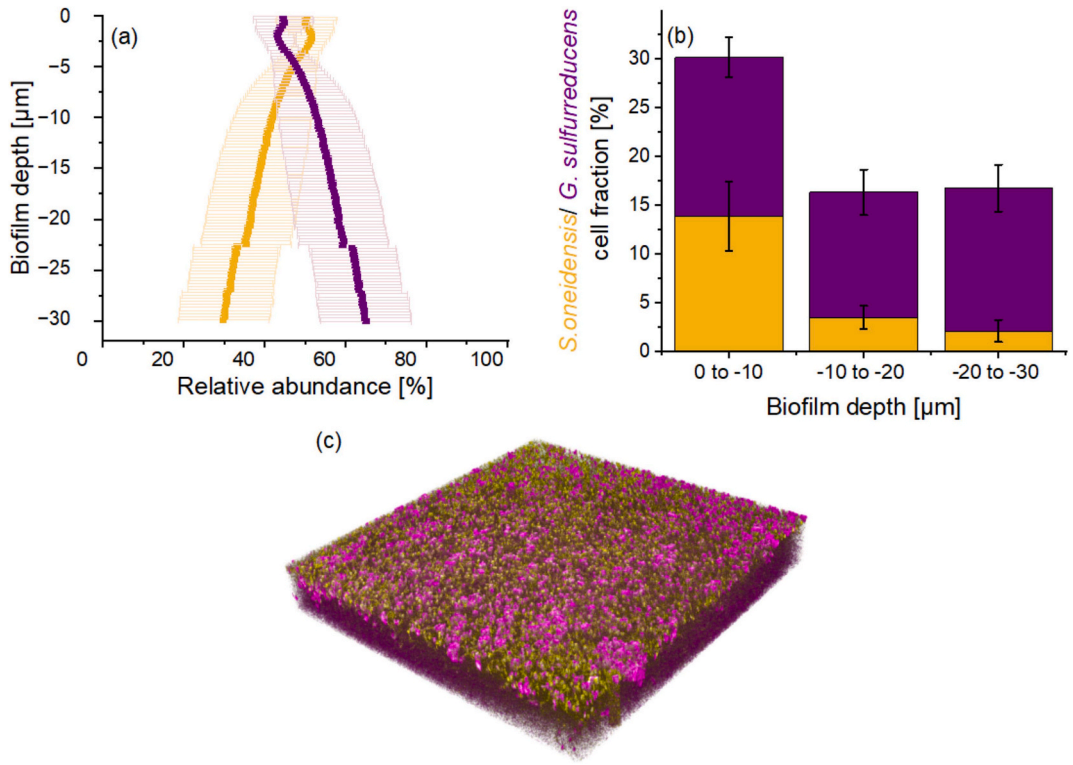

Fig. 5. Spatially resolved fluorescence in situ hybridization (FISH) analysis of *G. sulfurreducens* and *S. oneidensis* MR-1 ΔbpfD biofilms. The analysis was performed on a single mature biofilm sampled at the end of the experiment, in which the flow velocity was changed from 0.8 mm/s (Phase 1) to 0.2 mm/s (Phase 2). (a) The plotted ratio of the two species over biofilm depth, expressed as relative abundance between the two species. Here, 0 µm represents the outer biofilm layer, and increasing depth corresponds to closer proximity to the anode. (b) The cell fraction in the biofilm, expressed as a proportion of total imaged volume including non-cellular space. (c) An exemplary three-dimensional perspective of the biofilm.

experiment under a flow velocity of 0.2 mm/s. The two biofilms were exposed to different preceding flow conditions, however, as the present mutant was switched from 0.8 to 0.2 mm/s whereas the earlier wild type was maintained at a constant 0.2 mm/s, so this comparison serves as a same-platform reference rather than a fully matched control. Their study experienced dense, spatially organized biofilms with interconnected conductive networks, whereas the here studied mutant strain biofilms were more porous, less structured and exhibited a low cell fraction. Despite enrichment of *G. sulfurreducens* near the electrode, efficient current generation requires close spatial association between *G. sulfurreducens* and *S. oneidensis* to ensure sufficient acetate availability, especially in flow-through setups. This supports the hypothesis that, in mutant biofilms, lactate diffusion and corresponding electron delivery to electrode-proximal cells are likely limited by a thick, porous and poorly conductive upper layer, ultimately resulting in less acetate availability as well as unfavorable biofilm structure for *G. sulfurreducens*. In other words, the impaired biofilm-forming capacity of MR-1Δ*bpfD* likely promotes a heterogeneous structure and contributes to the low current density. The present study, however, does not resolve the biochemical mechanism linking *bpfD* regulation to current production at the molecular level. Direct analyses of EPS composition, BpfA localization, c-di-GMP levels, and flavin production would be needed to establish this link.

These results indicate that syntrophic electroactive biofilm responses to hydrodynamic perturbation include a gene-regulatory component that operates alongside the physical contributions of shear, substrate delivery, metabolite removal, boundary-layer thickness, and local mass transport. The deletion shows that *bpfD* is functionally important for biofilm structure and current, while its flow-dependent expression shows that the gene responds to flow. Together, the genetic and transcriptomic observations support a flow-regulated role, which neither would establish alone. In this two-species system, *S. oneidensis* shapes the spatial organization, conductivity, and current-generating capacity of the community through *bpfD*-dependent regulation of cell–cell connectivity, despite its minor share of transcriptional activity and of direct current production. This indicates that, in syntrophic electroactive biofilms, gene regulation by a less active partner can be an important factor for community-level performance.

4. Conclusions

This study shows that the architecture and electrochemical performance of syntrophic electroactive biofilms are governed not only by passive mechanical compression under flow, but also by an active, gene-regulated response to hydrodynamic shear. Importantly, while G. sulfurreducens monocultures were largely insensitive to the tested flow regimes, the S. oneidensis and G. sulfurreducens coculture exhibited pronounced velocity-dependent shifts in biofilm volume, porosity, and current output. This contrast highlights flow velocity as an important operational parameter in the investigated syntrophic model system. Transcriptomic profiling and targeted inactivation of bpfD identified S. oneidensis as a key contributor to biofilm architecture, whose shear-responsive regulation of cell–cell connectivity shapes community-level conductivity despite its minor contribution to transcriptional activity. These findings suggest that, in multispecies electroactive biofilms, the physiological response of non-Geobacter partners can influence overall biofilm performance. Accordingly, BESs designed to valorize substrates beyond acetate, such as lactate, glycerol, or other complex carbon sources requiring upstream fermentative or oxidative partners, may benefit from optimization strategies that also consider hydrodynamic conditions and partner-specific regulatory responses. Future studies using additional cocultures, flow conditions, and reactor configurations will be important to evaluate how broadly these principles apply to electroactive biofilm engineering.

CRediT authorship contribution statement

Mahshid Golalikhani: Writing – original draft, Visualization, Validation, Methodology, Investigation, Formal analysis, Data curation, Conceptualization. **Ahmed Elreedy:** Writing – review & editing, Writing – original draft, Visualization, Validation, Methodology, Investigation, Formal analysis. **Benjamin Fritz:** Validation, Investigation, Formal analysis, Data curation. **René Wurst:** Writing – review & editing, Formal analysis. **Christian Jonas Lapp:** Validation, Investigation, Formal analysis, Data curation. **Johannes Gescher:** Writing – review & editing, Supervision, Resources, Project administration, Methodology, Funding acquisition, Conceptualization.

Declaration of Generative AI and AI-assisted technologies in the writing process

During the preparation of this work the authors used ChatGPT-4 (OpenAI) in order to improve the readability and language of this manuscript. After using this tool, the authors reviewed and edited the content as needed and take full responsibility for the content of the published article.

Declaration of competing interest

The authors declare that they have no known competing financial interests or personal relationships that could have appeared to influence the work reported in this paper.

Acknowledgements

This work was financially supported by the Baden-Württemberg Ministry for the Environment, Climate and Energy Management, and the European Union (EU) within the framework of the European Regional Development Fund (ERDF) for the project KoalAplan (grant number: Bioök_2076413). We gratefully acknowledge funding from the Deutsche Forschungsgemeinschaft (priority program SPP2494, project no. 559358135). The authors would like to thank Berivan Akgün, Daniel Bauer, and Beatriz Souza for their support in carrying out the experiments.

Appendix A. Supplementary data

Supplementary data to this article can be found online at https://doi.org/10.1016/j.biortech.2026.135330.

Data availability

The data analyzed in this study are available within the article and its supplementary files or from the corresponding author upon request.

References

Alotaibi, G.F., 2021. Factors Influencing Bacterial Biofilm Formation and Development. Am. J. Biomed. Sci. Res. 12, 617–626. https://doi.org/10.34297/ajbsr.2021.12.001820.

Bauer, A., Wagner, M., Saravia, F., Bartl, S., Hilgenfeldt, V., Horn, H., 2019. In-situ monitoring and quantification of fouling development in membrane distillation by means of optical coherence tomography. J. Memb. Sci. 577, 145–152. https://doi.org/10.1016/j.memsci.2019.02.006.

Chao, L., Rakshe, S., Leff, M., Spormanna, A.M., 2013. PdeB, a cyclic di-GMP-specific phosphodiesterase that regulates Shewanella oneidensis MR-1 motility and biofilm formation. J. Bacteriol. 195, 3827–3833. https://doi.org/10.1128/JB.00498-13.

Edel, M., Sturm, G., Sturm-Richter, K., Wagner, M., Ducassou, J.N., Couté, Y., Horn, H., Gescher, J., 2021. Extracellular riboflavin induces anaerobic biofilm formation in Shewanella oneidensis. Biotechnol. Biofuels 14, 130. https://doi.org/10.1186/s13068-021-01981-3.

Elgamoudi, B.A., Starr, K.S., Korolik, V., 2022. Extracellular c-di-GMP plays a role in biofilm formation and dispersion of *Campylobacter jejuni*. Microorganisms 10. https://doi.org/10.3390/microorganisms10102030.

Fang, Y., Xiao, N., Chen, D., Field, R.W., Wu, J.J., Wang, B., 2023. Influence of shear stress on the intracellular bis-(3′-5′)-cyclic dimeric guanosine monophosphate (c-di-GMP) level within an MBR biofilm. Chem. Eng. Sci. 280, 118989. https://doi.org/10.1016/j.ces.2023.118989.

Feng, Q., Luo, L., Chen, X., Zhang, K., Fang, F., Xue, Z., Li, C., Cao, J., Luo, J., 2021. Facilitating biofilm formation of *Pseudomonas aeruginosa* via exogenous N-Acy-L-homoserine lactones stimulation: regulation on the bacterial motility, adhesive ability and metabolic activity. Bioresour. Technol. 341, 125727. https://doi.org/10.1016/j.biortech.2021.125727.

Flemming, H.C., 2016. Eps—then and now. Microorganisms 4, 41. https://doi.org/10.3390/microorganisms4040041.

Fritz, B., Lapp, C.J., Gescher, J., 2025. Influence of different transposon families on genomic stability of Shewanella oneidensis MR1. J. Microbial. Biotechnol. 18. https://doi.org/10.1111/1751-7915.70188.

Gao, L., Lu, X., Liu, H., Li, J., Li, W., Song, R., Wang, R., Zhang, D., Zhu, J., 2019. Mediation of extracellular polymeric substances in microbial reduction of hematite by shewanella oneidensismr-1. Front. Microbiol. 10, 1–12. https://doi.org/10.3389/fmicb.2019.00575.

Godain, A., Vogel, T.M., Fongarland, P., Haddour, N., 2024. Influence of shear stress on electroactive biofilm characteristics and performance in microbial fuel cells. Biosens. Bioelectron. 244. https://doi.org/10.1016/j.bios.2023.115806.

Gomes, L.C., Mergulhão, F.J.M., 2021. A selection of platforms to evaluate surface adhesion and biofilm formation in controlled hydrodynamic conditions. Microorganisms 9. https://doi.org/10.3390/microorganisms9091993.

Guo, Y., Liu, S., Tang, X., Wang, C., Niu, Z., Feng, Y., 2017. Insight into c-di-GMP regulation in anammox aggregation in response to alternating feed loadings. Environ. Sci. Technol. 51, 9155–9164. https://doi.org/10.1021/acs.est.6b06396.

Hengge, R., 2009. Principles of c-di-GMP signalling in bacteria. Nat. Rev. Microbiol. 7, 263–273. https://doi.org/10.1038/nrmicro2109.

Islam, M.A., Ehiraj, B., Cheng, C.K., Dubey, B.N., Khan, M.M.R., 2019. Biofilm revitalization using hydrodynamic shear stress for stable power generation in microbial fuel cell. J. Electroanal. Chem. 844, 14–22. https://doi.org/10.1016/j.jelechem.2019.05.013.

Jadhav, D.A., Chendake, A.D., Schievano, A., Pant, D., 2019. Suppressing methanogens and enriching electrogens in bioelectrochemical systems. Bioresour. Technol. 277, 148–156. https://doi.org/10.1016/j.biortech.2018.12.098.

Jadhav, G.S., Ghangrekar, M.M., 2009. Performance of microbial fuel cell subjected to variation in pH, temperature, external load and substrate concentration. Bioresour. Technol. 100, 717–723. https://doi.org/10.1016/j.biortech.2008.07.041.

Jones, A.-A.D., 2018. Exoelectrogenic Biofilm Growth in Shearing Flows. https://doi.org/1721.1/115610.

Jones, A.A.D., Buie, C.R., 2019. Continuous shear stress alters metabolism, mass-transport, and growth in electroactive biofilms independent of surface substrate transport. Sci. Rep. 9, 1–8. https://doi.org/10.1038/s41598-019-39267-2.

Kitayama, M., Koga, R., Kasai, T., Kouzuma, A., Watanabe, K., 2017. Structures, compositions, and activities of live Shewanella biofilms formed on graphite electrodes in electrochemical flow cells. Appl. Environ. Microbiol. 83. https://doi.org/10.1128/AEM.00903-17.

Klein, E., Wurst, R., Rehnlund, D., Gescher, J., 2024a. Elucidating the development of cooperative anode-biofilm-structures. Biofilm 7, 100193. https://doi.org/10.1016/j.bioflm.2024.100193.

Klein, E.M., Heintz, H., Wurst, R., Lapp, C.J., Edel, M., Hähl, H., Jacobs, K., Gescher, J., 2025. Tailored enzyme expression modifies Shewanella oneidensis biofilms and increases current density. N. Biotechnol. 89, 1–10. https://doi.org/10.1016/j.nbt.2025.05.006.

Klein, E.M., Heintz, H., Wurst, R., Schuldt, S., Hähl, H., Jacobs, K., Gescher, J., 2024b. Comparative analysis of the influence of BpfA and BpfG on biofilm development and current density in Shewanella oneidensis under oxic, fumarate- and anode-respiring conditions. Sci. Rep. 14, 1–12. https://doi.org/10.1038/s41598-024-73474-w.

Klein, E.M., Knoll, M.T., Gescher, J., 2023. Microbe–Anode Interactions: comparing the impact of genetic and material engineering approaches to improve the performance of microbial electrochemical systems (MES). Microb. Biotechnol. 1–24. https://doi.org/10.1111/1751-7915.14236.

Kokko, M., Epple, S., Gescher, J., Kerzenmacher, S., 2018. Effects of wastewater constituents and operational conditions on the composition and dynamics of anodic microbial communities in bioelectrochemical systems. Bioresour. Technol. 258, 376–389. https://doi.org/10.1016/j.biortech.2018.01.090.

Kolker, E., Picone, A.F., Galperin, M.Y., Romine, M.F., Higdon, R., Makarova, K.S., Kolker, N., Anderson, G.A., Qiu, X., Auberry, K.J., Babnigg, G., Beliaev, A.S., Edlefsen, P., Elias, D.A., Gorby, Y.A., Holzman, T., Klappenbach, J.A., Konstantinidis, K.T., Land, M.L., Lipton, M.S., McCue, L.A., Monroe, M., Pasa-Tolic, L., Pinchuk, G., Purvine, S., Serres, M.H., Tsapin, S., Zakrajsek, B.A., Zhu, W., Zhou, J., Larimer, F.W., Lawrence, C.E., Riley, M., Collart, F.R., Yates, J.R., Smith, R. D., Giometti, C.S., Nealson, K.H., Fredrickson, J.K., Tiedje, J.M., 2005. Global profiling of Shewanella oneidensis MR-1: expression of hypothetical genes and improved functional annotations. Proc. Natl. Acad. Sci. u. s. a. 102, 2099–2104. https://doi.org/10.1073/pnas.0409111102.

Kouzuma, A., Meng, X.Y., Kimura, N., Hashimoto, K., Watanabe, K., 2010. Disruption of the putative cell surface polysaccharide biosynthesis Gene SO3177 in Shewanella oneidensis MR-1 enhances adhesion to electrodes and current generation in microbial fuel cells. Appl. Environ. Microbiol. 76, 4151–4157. https://doi.org/10.1128/AEM.00117-10.

Kugaprasatham, S., Nagaoka, H., Ohgaki, S., 1992. Effect of turbulence on nitrifying biofilms at non-limiting substrate conditions. Water Res. 26, 1629–1638. https://doi.org/10.1016/0043-1354(92)90162-W.

Lin, R., Cheng, J., Zhang, J., Zhou, J., Cen, K., Murphy, J.D., 2017. Boosting biomethane yield and production rate with graphene: the potential of direct interspecies electron transfer in anaerobic digestion. Bioresour. Technol. 239, 345–352. https://doi.org/10.1016/j.biortech.2017.05.017.

Liu, S., Gunawan, C., Barraud, N., Rice, S.A., Harry, E.J., Amal, R., 2016. Understanding, monitoring, and controlling biofilm growth in drinking water distribution systems. Environ. Sci. Technol. 50, 8954–8976. https://doi.org/10.1021/acs.est.6b00835.

Mahto, K.U., Das, S., 2022. Bacterial biofilm and extracellular polymeric substances in the moving bed biofilm reactor for wastewater treatment: a review. Bioresour. Technol. 345, 126476. https://doi.org/10.1016/j.biortech.2021.126476.

Matsumoto, A., Koga, R., Kanaly, R.A., Kouzuma, A., Watanabe, K., 2021. Identification of a diguanylate cyclase that facilitates biofilm formation on electrodes by Shewanella oneidensis MR-1. Appl. Environ. Microbiol. 87, 1–11. https://doi.org/10.1128/AEM.00201-21.

Park, S., Sauer, K., 2022. Controlling Biofilm Development Through Cyclic di-GMP Signaling, in: Advances in Experimental Medicine and Biology. Adv Exp Med Biol, pp. 69–94. https://doi.org/10.1007/978-3-031-08491-1_3.

Pham, H.T., Boon, N., Aelterman, P., Clauwaert, P., De Schamphelaire, L., Van Oostveldt, P., Verbeken, K., Rabaey, K., Verstraete, W., 2008. High shear enrichment improves the performance of the anodophilic microbial consortium in a microbial fuel cell. Microb. Biotechnol. 1, 487–496. https://doi.org/10.1111/j.1751-7915.2008.00049.x.

Pizzi, F., Peters, F., Sorribes, E., Marín-Beltrán, I., Romera-Castillo, C., Grau, J., Rahmani, M., Jofre, L., Capuano, F., 2025. Modulation of biofilm growth by shear and fluctuations in turbulent environments. Sci. Rep. 15, 1–21. https://doi.org/10.1038/s41598-025-95822-0.

Rago, L., Baeza, J.A., Guisasola, A., 2016. Increased performance of hydrogen production in microbial electrolysis cells under alkaline conditions. Bioelectrochemistry 109, 57–62. https://doi.org/10.1016/j.bioelechem.2016.01.003.

Tan, C.H., Oh, H.S., Sheraton, V.M., Mancini, E., Joachim Loo, S.C., Kjelleberg, S., Sloot, P.M.A., Rice, S.A., 2020. Convection and the extracellular matrix dictate inter- and intra-biofilm quorum sensing communication in environmental systems. Environ. Sci. Technol. 54, 6730–6740. https://doi.org/10.1021/acs.est.0c00716.

Tang, K., Li, S., Luo, Y., Feng, W., Zhang, Z., Wang, L., Zhao, H., Chen, X., Li, X., Wu, Z., 2025. Integrating metagenomics and untargeted metabolomics to analyze the relationship between microbial dynamics and non-volatile metabolomic profiles in plant-derived microbial fuel cells (MFCs). RSC Adv. 15, 19582–19597. https://doi.org/10.1039/d5ra01080b.

Thormann, K.M., Duttler, S., Saville, R.M., Hyodo, M., Shukla, S., Hayakawa, Y., Spormann, A.M., 2006. Control of formation and cellular detachment from Shewanella oneidensis MR-1 biofilms by cyclic di-GMP. J. Bacteriol. 188, 2681–2691. https://doi.org/10.1128/JB.188.7.2681-2691.2006.

Van Loosdrecht, M.C.M., Heijnen, J.J., Eberl, H., Kreft, J., Picioreanu, C., 2002. Mathematical modelling of biofilm structures Antonie Van Leeuwenhoek. Int. J. Gen. Mol. Microbiol. 81, 245–256. https://doi.org/10.1023/A:1020527020464.

Wagner, M., Horn, H., 2017. Optical coherence tomography in biofilm research: a comprehensive review. Biotechnol. Bioeng. 114, 1386–1402. https://doi.org/10.1002/bit.26283.

Wang, S., Zhu, H., Zheng, G., Dong, F., Liu, C., 2022. Dynamic changes in biofilm structures under dynamic flow conditions. Appl. Environ. Microbiol. 88. https://doi.org/10.1128/aem.01072-22.

Xiao, W., Xu, G., Li, G., 2021. Role of shear stress in biological aerated filter with nanobubble aeration: performance, biofilm structure and microbial community. Bioresour. Technol. 325, 124714. https://doi.org/10.1016/j.biortech.2021.124714.

Yang, J., Cheng, S., Li, C., Sun, Y., Huang, H., 2019. Shear stress affects biofilm structure and consequently current generation of bioanode in microbial electrochemical systems (MESS). Front. Microbiol. 10, 1–8. https://doi.org/10.3389/fmicb.2019.00398.

Zhou, G., Yuan, J., Gao, H., 2015. Regulation of biofilm formation by BpfA, BpfD, and BpfG in Shewanella oneidensis. Front. Microbiol. 6, 790. https://doi.org/10.3389/fmicb.2015.00790.